Supporting Information

PtAu alloying-modulated hydroxyl and substrate adsorptions for glycerol electrooxidation to C$_3$ products

Yan Li [a], Xinfa Wei [c], Rui Pan [e], Yue Wang [a], Juanjuan Luo [a], Lanxin Li [a], Lisong Chen [a,d*], Jianlin Shi [b*]*

a. *State Key Laboratory of Petroleum Molecular & Process Engineering, Shanghai Key Laboratory of Green Chemistry and Chemical Processes, School of Chemistry and Molecular Engineering, East China Normal University, Shanghai 200062, China. E-mail: lschen@chem.ecnu.edu.cn*

b. *Shanghai Institute of Ceramics, Chinese Academy of Sciences, Shanghai 200050, P. R. China. E-mail: jlshi@mail.sic.ac.cn*

c. *Qingdao Institute of Bioenergy and Bioprocess Technology, Chinese Academy of Sciences, Shandong Energy Institute, Qingdao New Energy Shandong Laboratory, Qingdao 266101, China. E-mail: weixf2024@qibebt.ac.cn*

d. *Institute of Eco-Chongming, Shanghai 202162, China.*

e. *SEU-FEI Nano-Pico Center, Key Laboratory of MEMS of Ministry of Education, Southeast University, Nanjing, 210096 P. R. China.*

Experimental Procedures

Chemicals

H_2PtCl_6 $6H_2O$ (RG), $HAuCl_4$ $3H_2O$ (RG), maleic acid (99%, RG, grade) and deuterated water (D_2O) were bought from Adamas Reagent Co., Ltd. (Tansoole). Pluronic F127 ($PEO_{100}PPO_{65}PEO_{100}$) was bought from Macklin. Glycerol (AR) was bought from Chinese medicine reagent. Ethylene glycol (AR) and 1,2-propanediol (AR) were purchased from general reagent. All chemicals were used as received without any further purification. Deionized water (DIW) was used in all experiments.

Material synthesis

The hp-PtAu/NF electrode was prepared via a chemical deposition method. Prior to the deposition, a piece of Ni foam (named as NF) was pretreated with 3 M HCl, ethanol and DIW in an ultrasonic cleaner for 15 min, respectively. Then, 0.6 mL of H_2PtCl_6 $6H_2O$ (20 mM), 2.4 mL of $HAuCl_4$ $3H_2O$ (20 mM), 30 mg Pluronic F127, 10 µl of ethanol and 25 µl of HCl (6 M) were mixed in a glass bottle under stirring for 10 min to obtain a uniform aqueous solution. Subsequently, the treated NF was immersed in the above mixture at 50 °C for 6 h. At the end of the reaction, the products based on Ni foam were washed with DIW and ethanol for several times to remove unreacted residues (donated as hp-PtAu/NF or Pt_1Au_4/NF, mass loading: 3.33 mg_{Pt+Au} cm^{-2}). The Pt/NF, Pt_9Au_1/NF, Pt_4Au_1/NF, Pt_1Au_1/NF, Pt_1Au_4/NF, Pt_1Au_9/NF and Au/NF were fabricated by

changing the molar ratio of initially added Pt to Au while keeping the total amount of metal precursors unchanged, and the Pt-to-Au molar ratio of these prepared samples determined by inductively coupled plasma optical emission spectrometry (ICP-OES) were 100 : 0, 94.6 : 5.4, 84.0 : 16.0, 71.6 : 28.4, 29.7 : 70.3, 18.8 : 81.2 and 0 :100, respectively.

Characterizations

X-ray diffraction (XRD) was measured on a Rigaku D/MAX 2550 diffractometer using a Cu Ka source (l = 1.5418 Ǻ). X-ray photoelectron spectra (XPS) were collected on X-ray photoelectron spectroscopy (XPS, AXIS SUPRA) with Mg Kα radiation source (hv=1253.6eV). The microscopic features of the catalysts were performed using scanning electron microscope (SEM, ZEISS Gemini 450, 3 kV) and transmission electron microscope (TEM, JEOL JEM-F200, 200 kV). ICP-OES results were collected on an Agilent 700 Series instrument.

In situ Fourier Transform Infrared (FTIR) measurements were performed on a Linglu instruments FTIR cell mounted on a Pike Veemax III ATR, and spectra were recorded on a Thermo Fisher IS 50 spectrometers with MCT detector. Electrochemical measurements were recorded on a CHI 760E electrochemical workstation in a three-electrode configuration at room temperature, using Hg/HgO electrode and Pt wire as reference and counter electrode, respectively. 1 M KOH with 0.5 M glycerol was utilized as electrolyte and was purged with nitrogen before tests.

In situ Raman measurements were performed on a Renishaw inVia Reflex Raman microscope with a 532 nm laser as excitation source and a CHI 760E electrochemical workstation. The cell was made by Teflon shell with a quartz window between the sample and objective. The reference and counter electrodes were Ag/AgCl electrode and Pt wire electrode, respectively. The self-supported working electrodes were inserted through the wall of the cell to keep the plane to the incident laser and the Raman spectra were recorded at different potentials in 1M KOH with 0.5 M glycerol.

Electrochemical measurements

All electrochemical measurements were performed in 1 M KOH electrolyte at room temperature on a BioLogic VSP-300 electrochemical workstation. The measurements for alcohol oxidation and HER were performed in a three-electrode cell utilizing Hg/HgO and graphite rod as the counter and reference electrode, respectively. The measured potentials against Hg/HgO were converted to reversible hydrogen electrode (RHE) according to the following equation (1):

$$E_{RHE} = E_{Hg/HgO} + 0.059 \text{ pH} + 0.098 \tag{1}$$

The overall electrolysis was carried out in a two-electrode system, and the Pt_1Au_4/NF and Pt_1Au_1/NF were used as anode and cathode. The area of the working electrode in the electrolyte was fixed at 1×0.5 cm^2 and all current densities were based on the geometrical area of the electrode unless specified. Cyclic voltammetry (CV) and linear scan voltammetry (LSV) curves of the electrocatalysts were measured at a scan rate of 50 and 2 mV s^{-1} without iR-

compensation unless specified. The specified iR compensation was auto-compensated by the electrochemical workstation and the iR compensation value was controlled as 85%. Electrochemically surface area (ECSA) was calculated by evaluating the electrochemical double layer capacitances (Cdl) of as-prepared samples based on equation (2):

$$ECSA = S\frac{C_{dl}}{C_s}$$
(2)

where C_{dl} was measured from the scan-rate-dependent CVs in the potential region without faradaic process. S represents the actual surface area of the electrode. C_s is the specific capacitance of a flat standard electrode, which is generally considered to be in the range of 20–60 μF cm^{-2}. In this work, the value of C_s is estimated to be 60 μF cm^{-2}. In-situ electrochemical impedance measurements (EIS) were performed in a frequency range from 10^5 to 10^{-2} Hz with an amplitude of 10 mV. The apparent activation energies for the GOR in 1M KOH with 0.5 M glycerol were determined according to the Arrhenius equation (3)[1]:

$$Ea = \frac{dlogj_0}{d(1/T)}$$
(3)

Where Ea is the apparent activation energy for GOR on the electrocatalyst, and j_o is the exchange current density.

Product quantification.

The chronoamperometry testing at varied potentials was conducted to determine the products of alcohol oxidations and HER. The liquid products at anode were

detected by nuclear magnetic resonance (NMR) spectrometer (AVANCE III HD500). A 500 µl sample after electrochemical reaction was collected and mixed with 100 µl D_2O for products quantification, and maleic acid was used as an internal standard. The cathodic H_2 was examined by a gas chromatograph (Ramiin GC2060) equipped with a packed column and a thermal conductivity detector, quantified by the external standard method (**Figure S38**).

The selectivity (%) of products was calculated by the following equations (4):

$$\text{Selectivity}(\%) = \frac{\text{n (product)}}{\text{n (consumed glycerol)}} \times 100\%$$

(4)

The Faradaic efficiency (%) of the products was calculated by the following equations (5):

$$\text{FE}(\%) = \frac{n(\text{product})}{Q_{tot}/(Z \times F)} \times 100\%$$

(5)

Where Q_{tot} is the quantity of total electric charge, z is the number of electrons per reaction, F is the Faraday constant (F = 96485 C mol^{-1}).

Computational Details

All electronic structure calculations are performed via the Vienna Ab-initio Simulation Package (VASP) based on density functional theory (DFT)[2]. The exchange-correlation energies are approximated using the Perdew, Burke, and Erzenhorf (PBE) approximation including a non-local van der Waals correction[3].

All calculations are performed using a plane-wave basis (plane-wave cutoff of 450 eV) with projected augmented wave (PAW) method. The Pt (111) and $Au_7Pt_3(111)$ surface was modeled by a supercell slab of 64 atoms with four atom layers in agreement with the TEM results, and a vacuum region of 20 Å was set to avoid artificial interactions. A Monkhorst-Pack k-point mesh of 2 x 2 x 1 was set. The convergence of energy was set at 10^{-5} eV and that of forces for geometry optimizations was set to 0.02 eV/Å.

To explore the geometry and morphology change of the glycerol on Pt and PtAu alloy during reaction conditions, Ab initio molecular dynamics (AIMD) simulations were carried out in the canonical (NVT) ensemble employing Nosé−Hoover thermostats[4] for at least 10 ps with a time step of 1 fs at 300 K. An implicit solvent model VASPSol[5] for canonical simulations was used to describe the electrochemical environment.
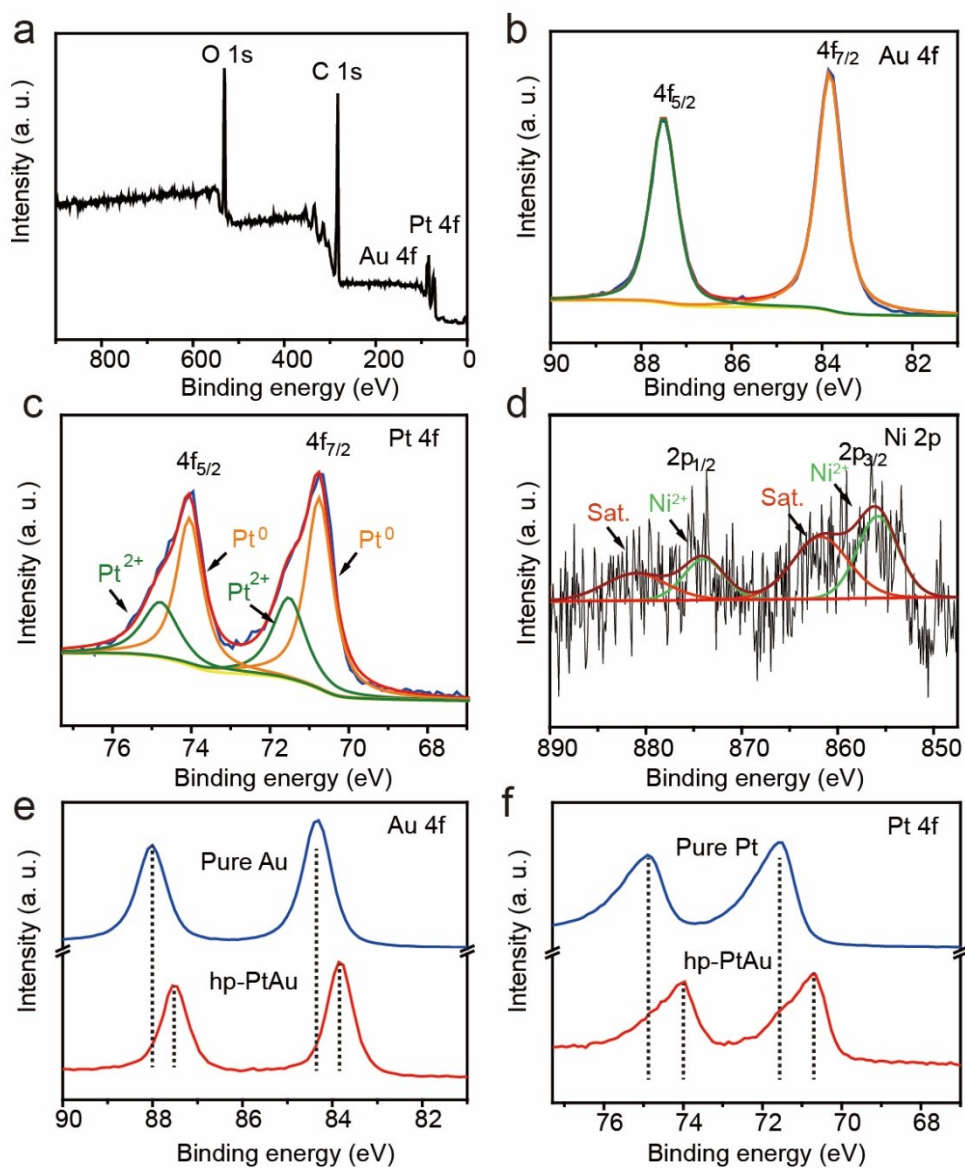
Figure S1. XPS analyses of the hp-PtAu/NF. (a) XPS survey spectrum and (b-c) high-resolution XPS spectra of hp-PtAu/NF: (b) Au 4f, (c) Pt 4f and (d) Ni 2p. (e) Pt 4f XPS spectra of hp-PtAu and pure Au. (f) Au 4f XPS spectra of hp-PtAu and pure Pt.
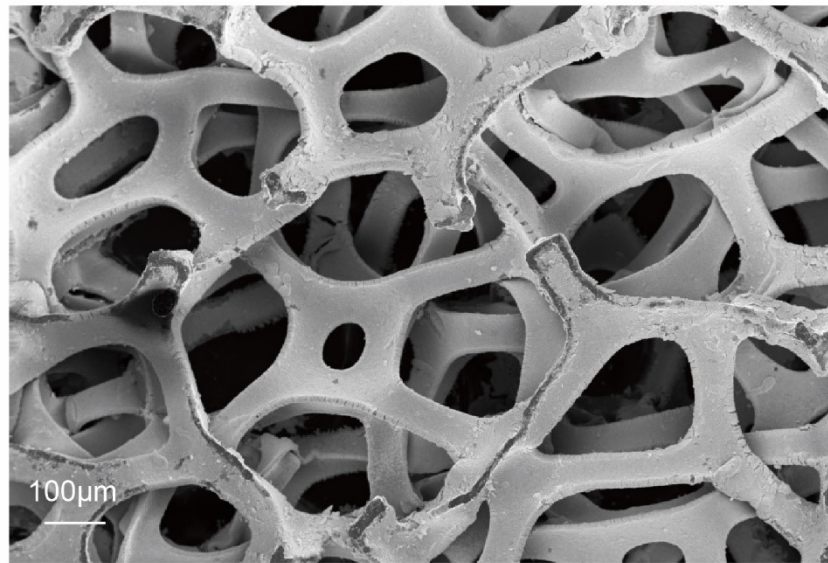
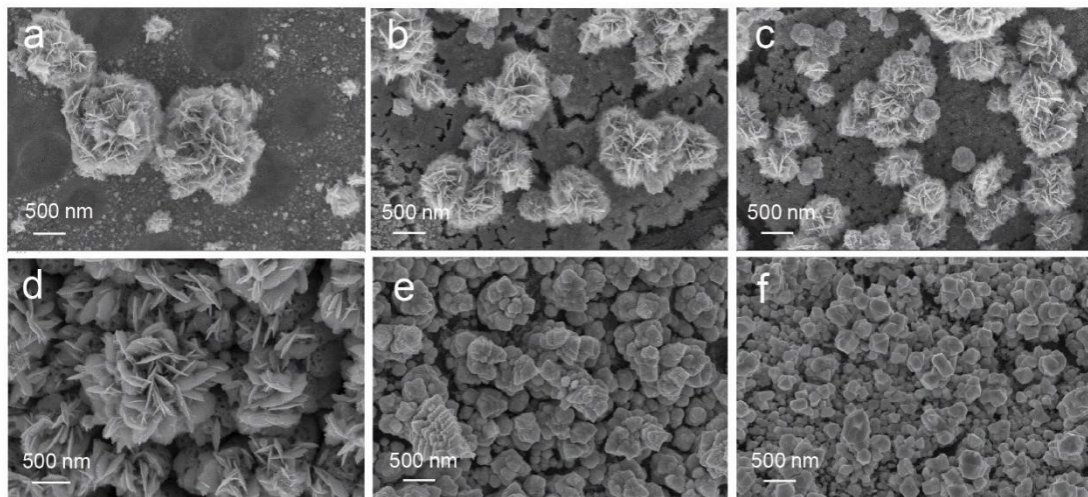**Figure S2.** SEM image of hp-PtAu/NF at low magnification.

Figure S3. SEM images of (a) Pt/NF, (b) Pt_9Au_1/NF, (c) Pt_4Au_1/NF, (d) Pt_1Au_1/NF, (e) Pt_1Au_9/NF and (f) Au/NF.
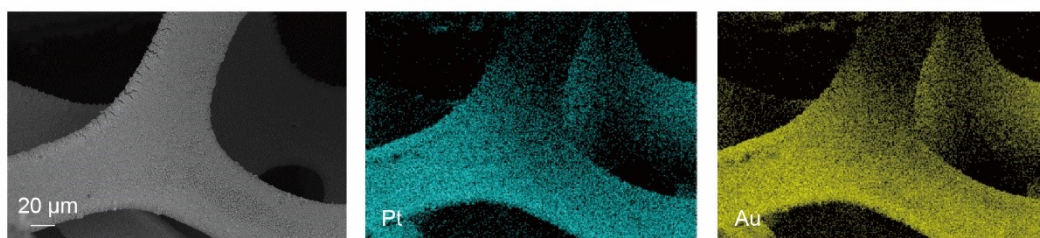
Figure S4. SEM image of hp-PtAu/NF and corresponding EDX mapping.
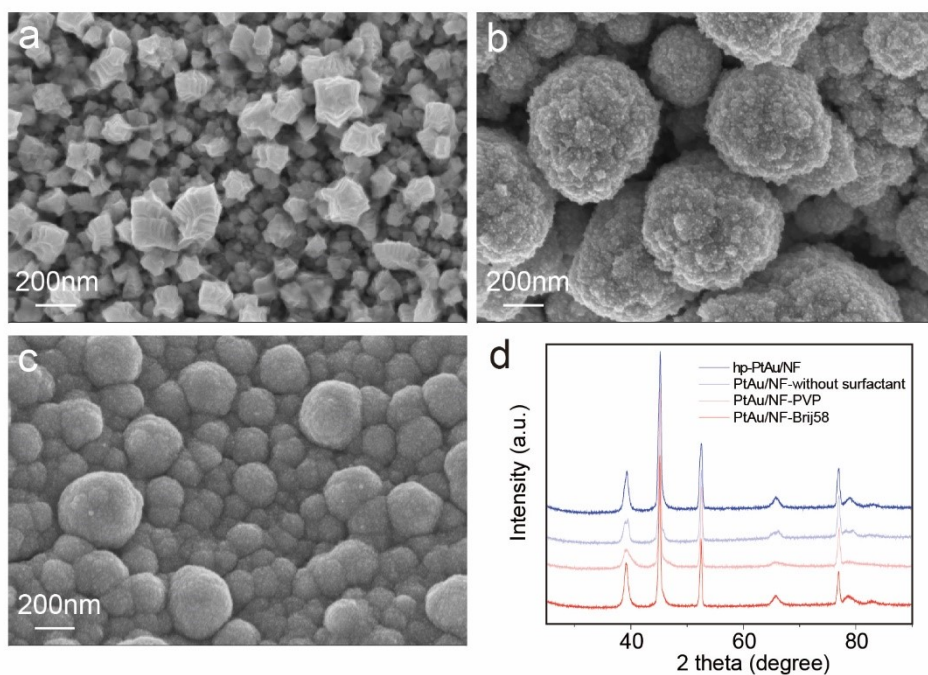
Figure S5. SEM images of as-prepared PtAu/NF using (a) no surfactants, (b) PVP and (c) Brij58. (d) XRD patterns of various catalysts.
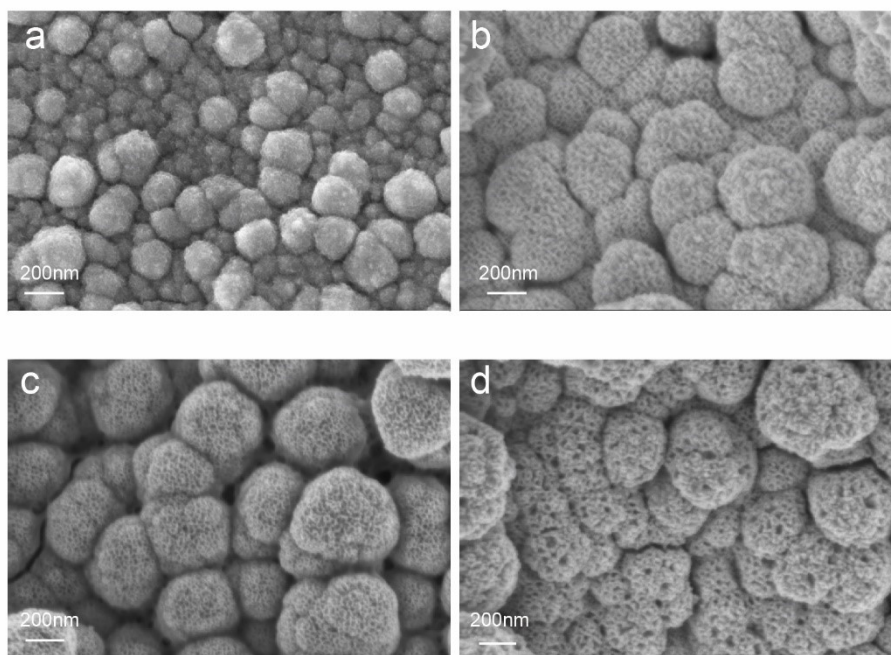

Figure S6. SEM images of hp-PtAu/NF obtained by reactions for different time periods of (a) 1 min, (b) 1 h, (c) 3 h and (d) 9 h.
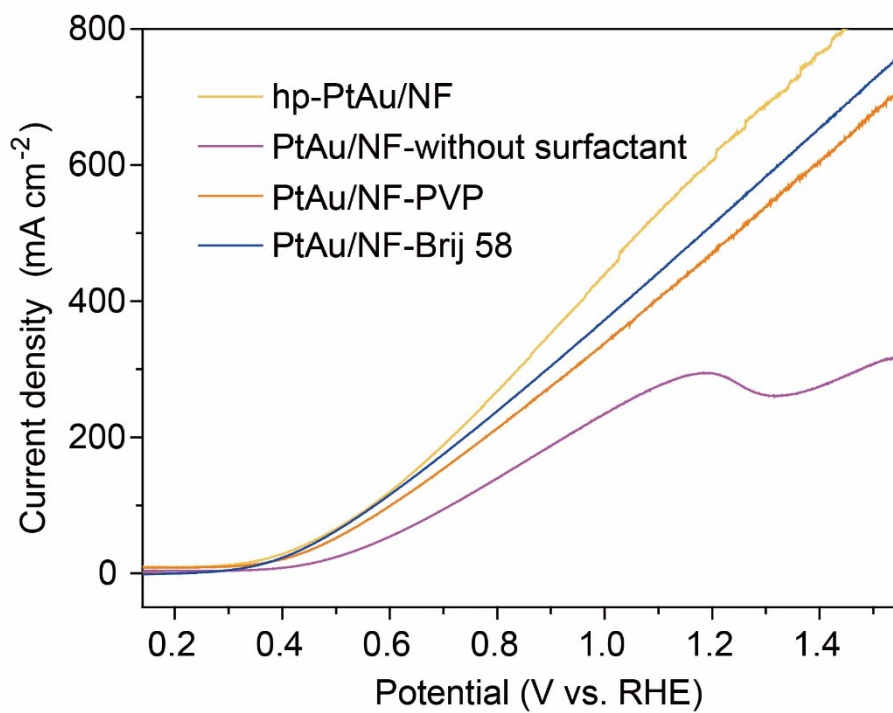
Figure S7. LSV curves of various PtAu/NF in 1 M KOH containing 0.5 M glycerol at the scan rate of 2 mV s^{-1}.
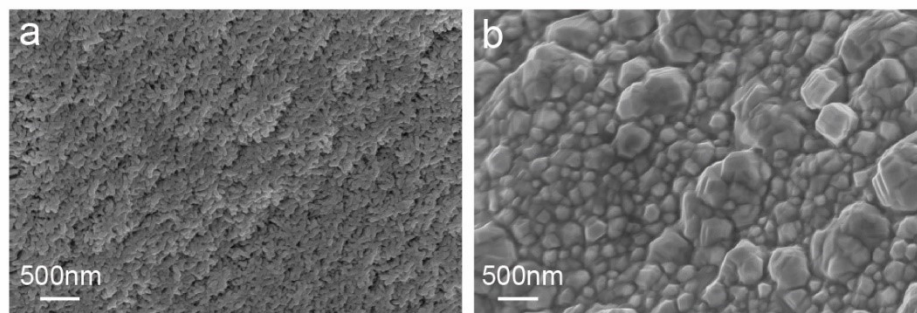

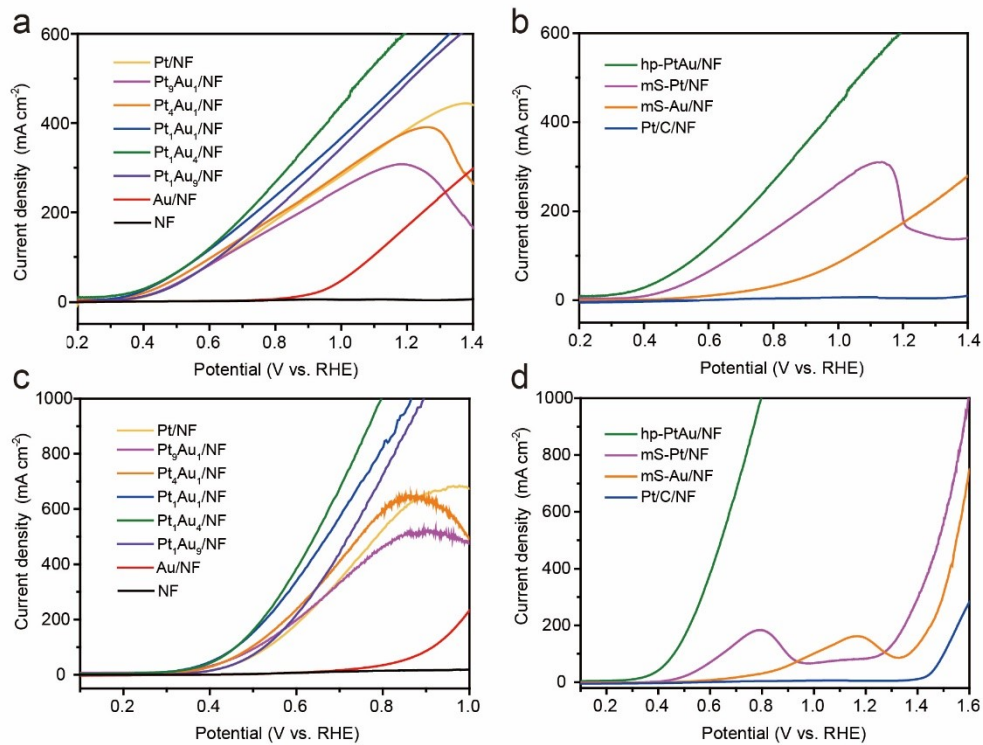**Figure S8.** SEM images of (a) mS-pt/NF and (b) mS-Au/NF prepared by magnetron sputtering.

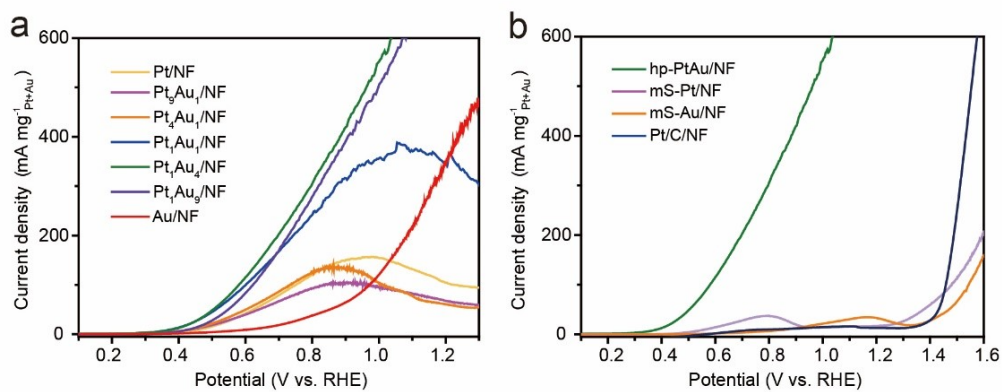**Figure S9.** LSV curves of various catalysts for GOR without (a, b) and with (c, d) *iR*-correction.

Figure S10. Mass activities of various catalysts for GOR (with *iR*-correction).
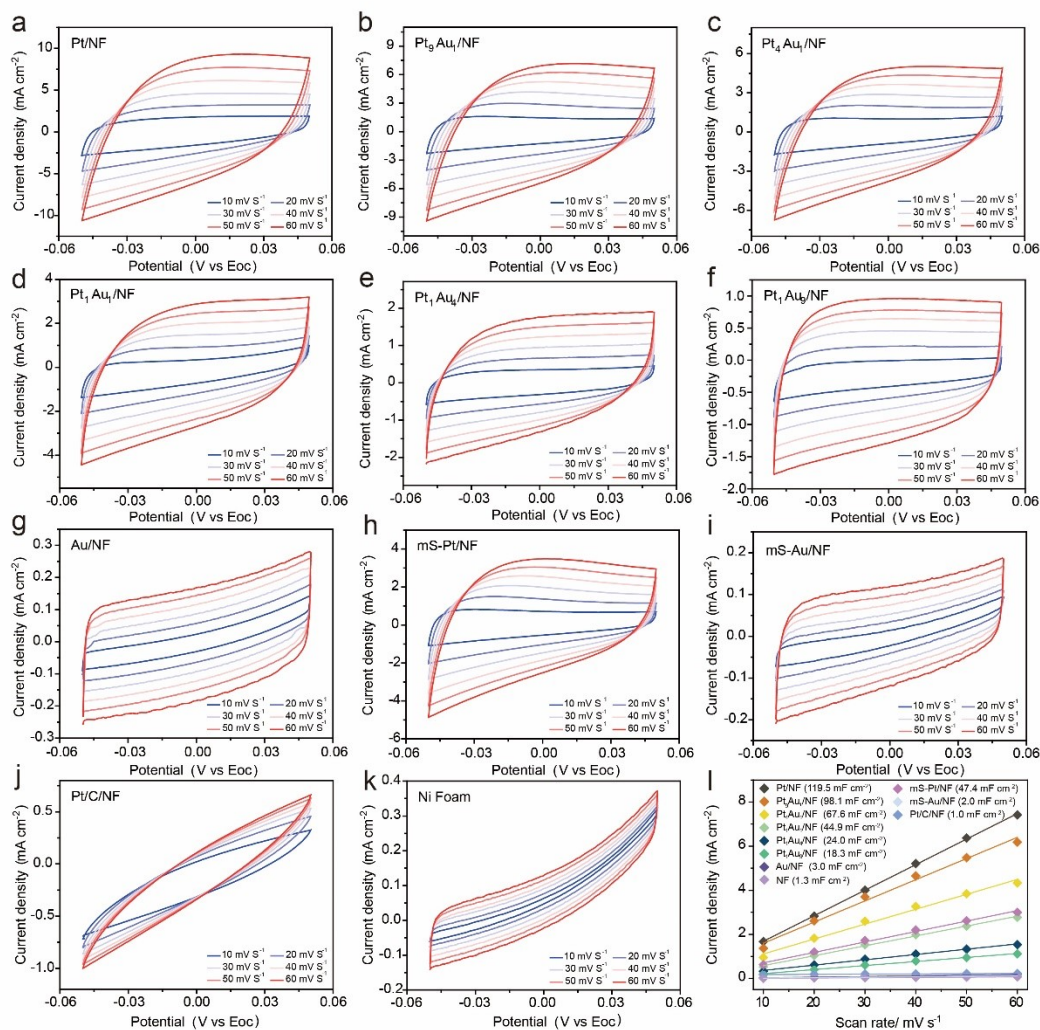
Figure S11. Electrochemical surface area (ECSA) tests of various catalysts in 1 M KOH containing 0.5 M glycerol. Electrochemical cyclic voltammetry scans recorded for (a) Pt/NF, (b) Pt_9Au_1/NF, (c) Pt_4Au_1/NF, (d) Pt_1Au_1/NF, (e) Pt_1Au_4/NF, (f) Pt_1Au_9/NF, (g) Au/NF, (h) mS-Pt/NF, (i) mS-Au/NF, (j) Pt/C/NF and (k) pure Ni foam. Eoc $_{Pt/NF}$ = -0.760 V, Eoc $_{Pt9Au1/NF}$ = -0.740 V, Eoc $_{Pt4Au1/NF}$ = -0.730 V, Eoc $_{Pt1Au1/NF}$ = -0.717 V, Eoc $_{Pt1Au4/NF}$ = -0.836 V, Eoc $_{Pt1Au9/NF}$ = -0.825 V, Eoc $_{Au/NF}$ = -0.498 V, Eoc $_{mS-Pt/NF}$ = -0.699 V, Eoc $_{mS-Au/NF}$ = -0.659 V, Eoc $_{Pt/C/NF}$ = -0.794 V. (l) Linear fittings of the capacitive currents versus cyclic voltammetry scans for these catalysts. The corresponding ECSA values for Pt/NF, Pt_9Au_1/NF, Pt_4Au_1/NF, Pt_1Au_1/NF, Pt_1Au_4/NF, Pt_1Au_9/NF, Au/NF, mS-Pt/NF, mS-Au/NF, Pt/C/NF and pure Ni foam are 946.5 cm^2, 801.0 cm^2, 552.1 cm^2, 366.5 cm^2, 196.2 cm^2, 149.5 cm^2, 24.3 cm^2, 386.9 cm^2, 16.4, 8.5 cm^2 and 11.0 cm^2, respectively.
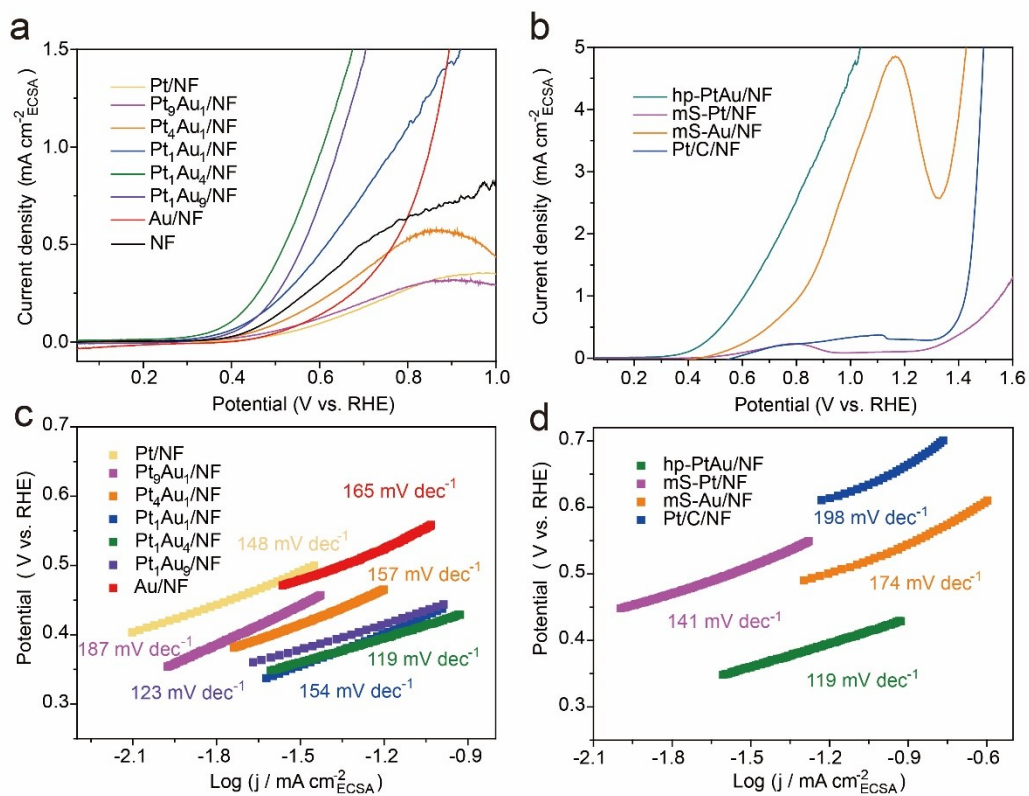
Figure S12. (a-b) ECSA-normalized LSV curves and (c-d) corresponding Tafel slopes of various materials (with *iR*-correction).
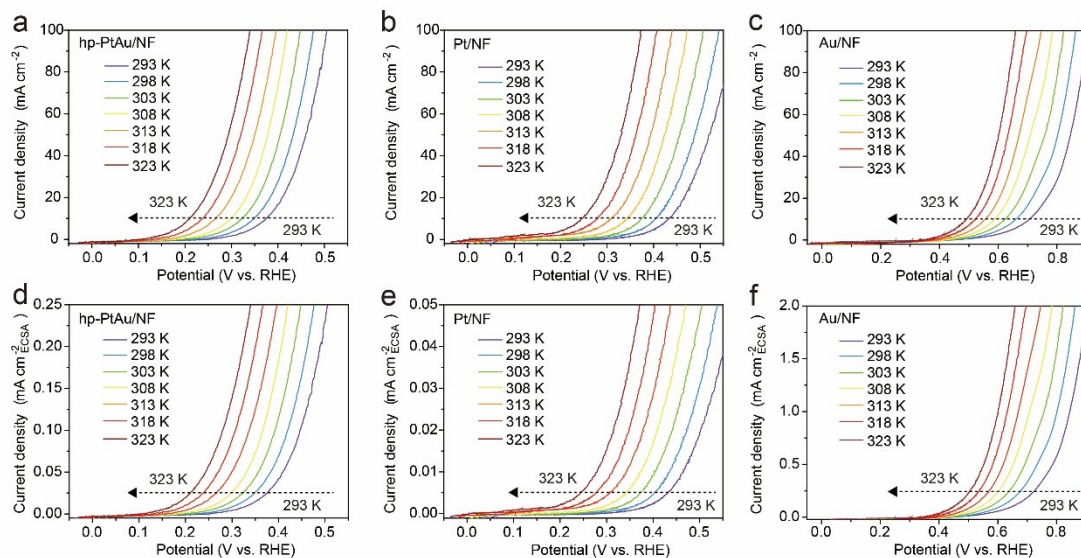
Figure S13. (a-c) LSV curves of hp-PtAu/NF, Pt/NF and Au/NF at different temperatures from 293 K to 323 K. (d-f) ECSA-normalized LSV curves of Pt/NF, hp-PtAu/NF and Au/NF at different temperatures from 293 K to 323 K (with *iR*-correction).
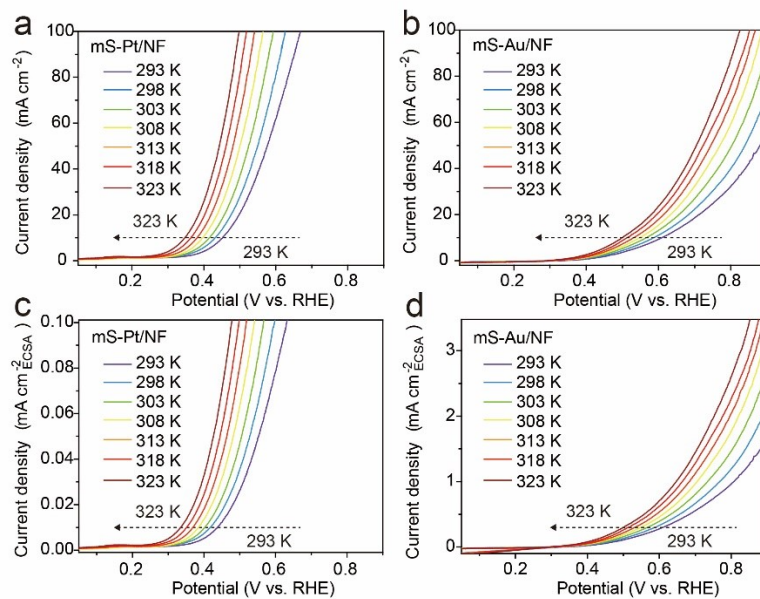

Figure S14. (a-c) LSV curves of mS-Pt/NF and mS-Au/NF at different temperatures from 293 K to 323 K. (d-f) ECSA-normalized LSV curves of mS-Pt/NF and mS-Au/NF at different temperatures from 293 K to 323 K (with *iR*-correction).
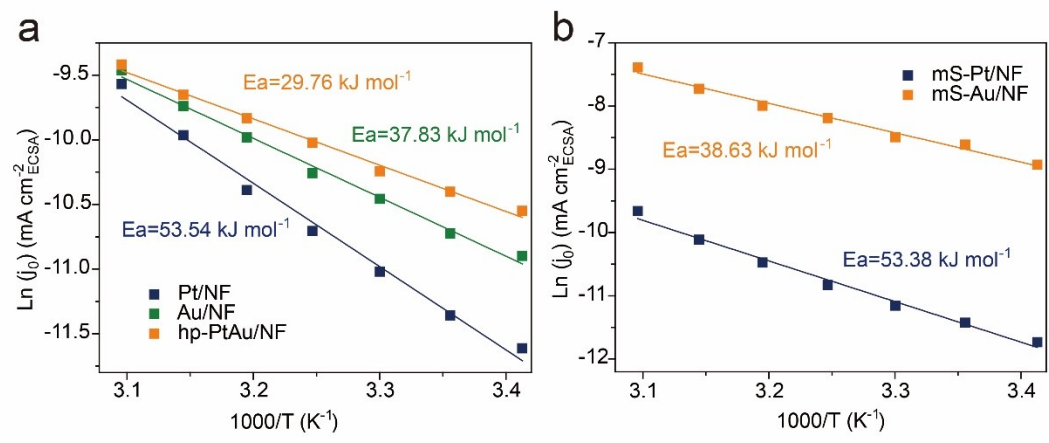
Figure S15. Arrhenius plots for (a) Pt/NF, Au/NF, hp-PtAu/NF, (b) mS-Pt/NF and mS-Au/NF over the temperature range of 293–323 K.
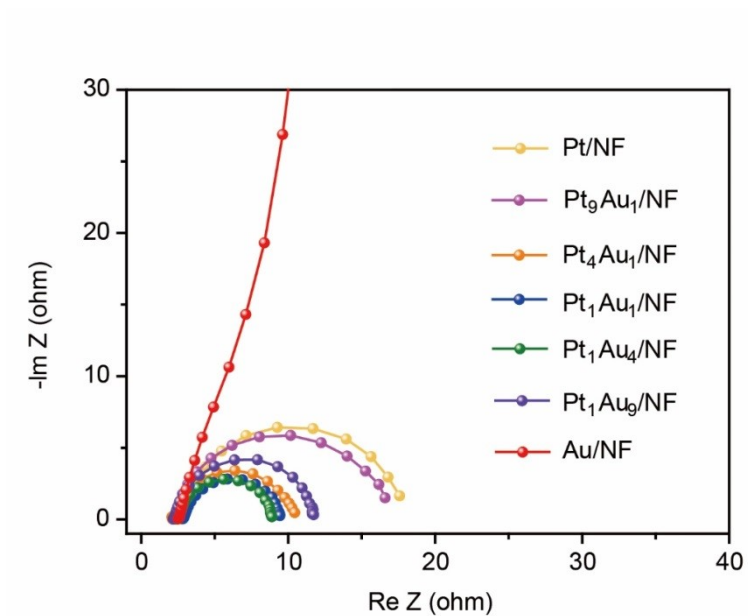
Figure S16. Nyquist plots of various catalysts for glycerol oxidation in 1.0 M KOH with 0.5 M glycerol.
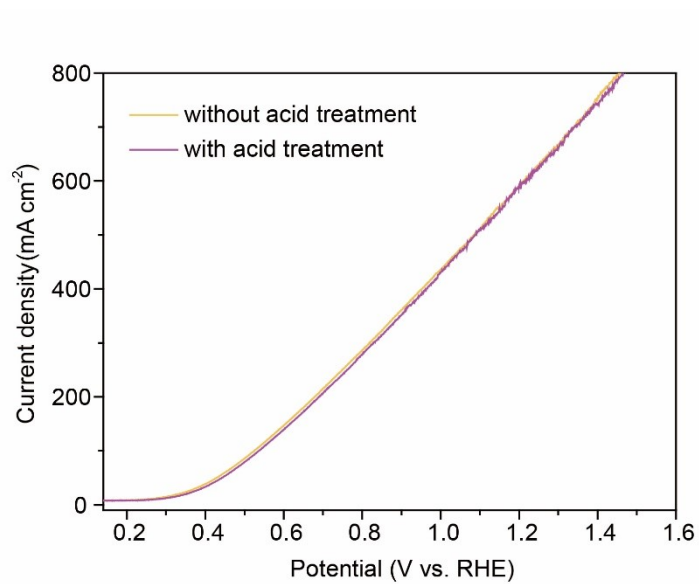
Figure S17. LSV curves of hp-PtAu/NF with and without acid treatment.

Figure S18. (a) Product selectivity for hp-PtAu/NF electrode in relation to applied potential. (b) C_3 productivity and selectivity for hp-PtAu/NF electrode in relation to applied potential.
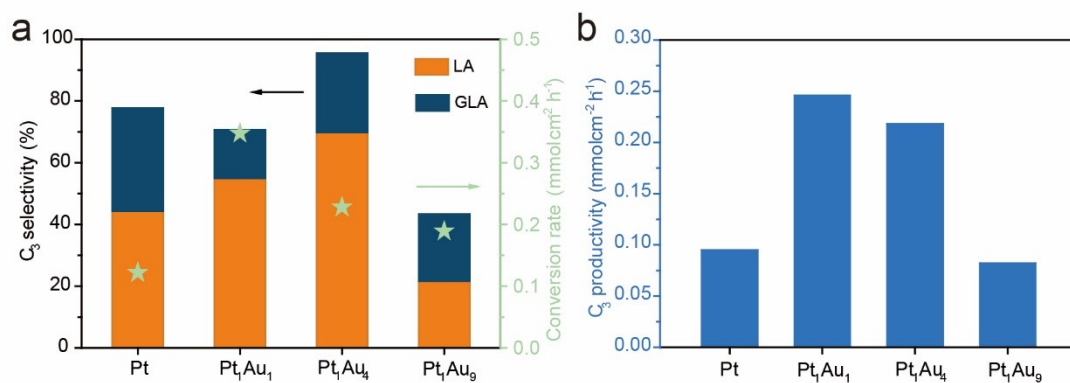
Figure S19. (a) Glycerol conversion rate and C_3 selectivity at 0.4 V vs. RHE over different catalysts. (b) C_3 productivity at 0.4 V vs. RHE over different catalysts.
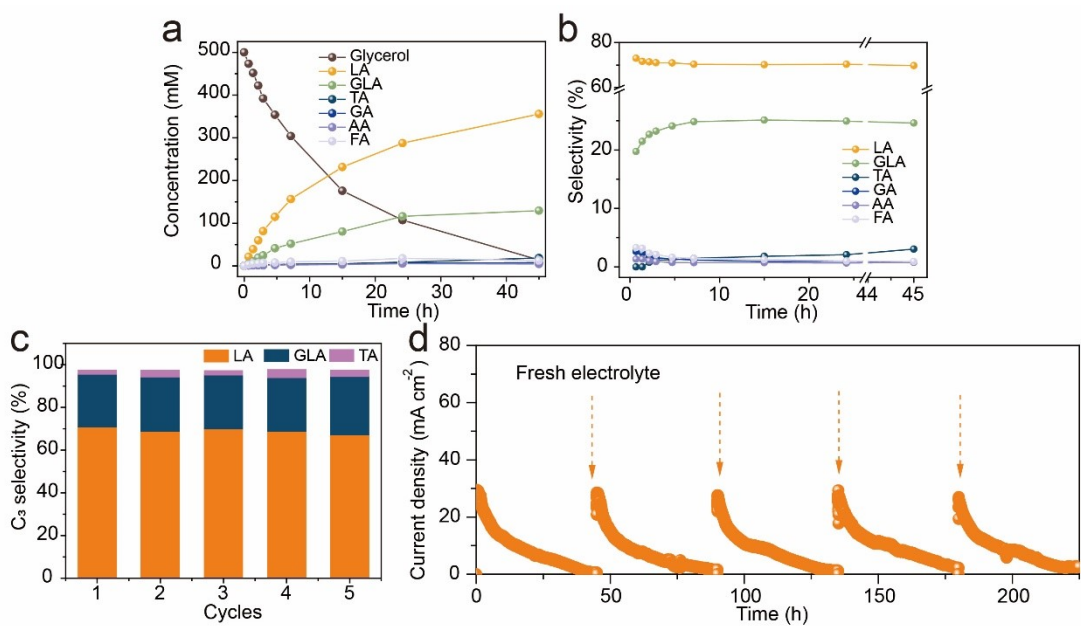
Figure S20. (a) Concentrations of glycerol and its oxidation products as functions of time at a potential of 0.4 V vs RHE. (b) Selectivities as functions of time at a potential of 0.4 V vs RHE. (c) Selectivity of hp-PtAu/NF for C_3 products for five successive electrolysis cycles. (d) I-t curves of hp-PtAu/NF for five successive electrolysis cycles at 0.4 V vs RHE. Electrode area: 3 cm^2. Electrolyte volume: 20 mL.
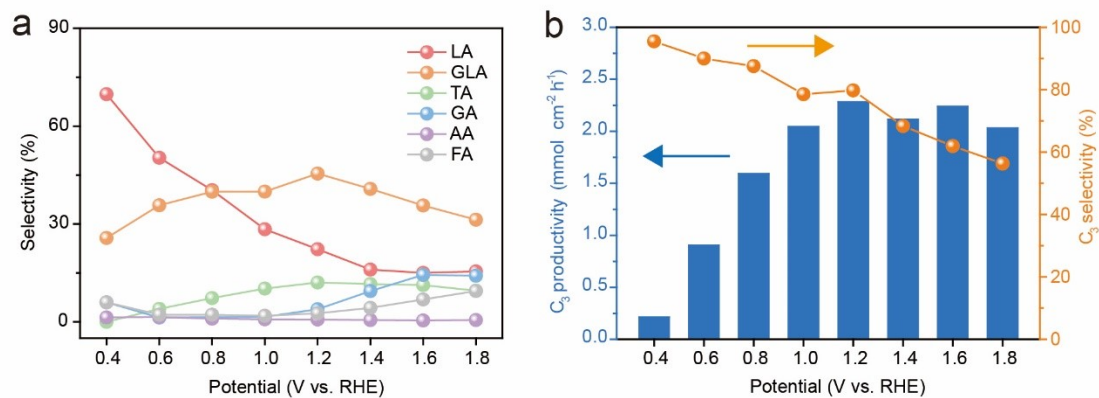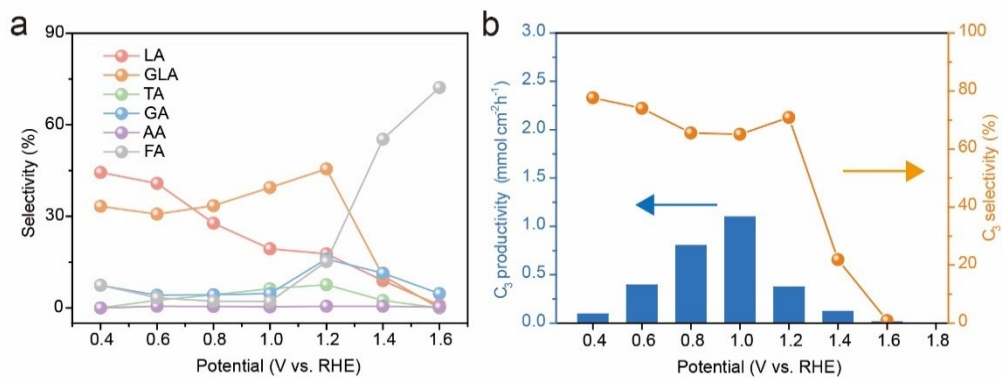
Figure S21. (a) Product selectivity for Pt/NF electrode in relation to applied potential. (b) C_3 productivity and selectivity for Pt/NF electrode in relation to applied potential.
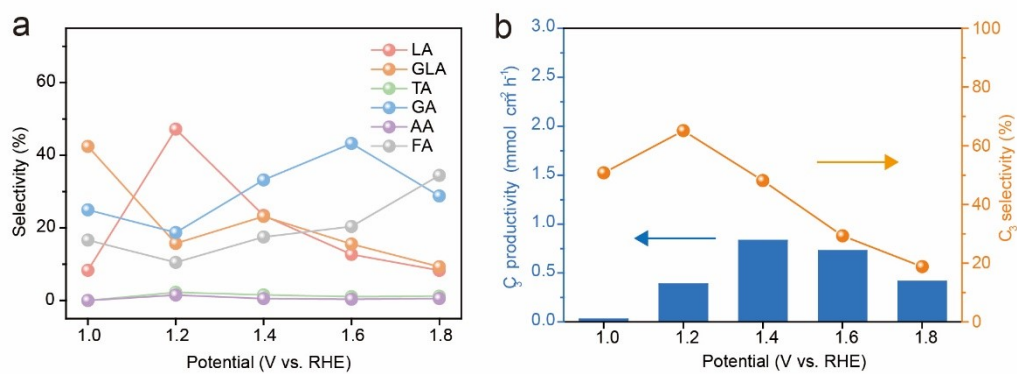
**Figure S22.** (a) Product selectivity at varied applied potentials over Au/NF electrode. (b) C_3 productivity and selectivity at varied applied potentials over Au/NF electrode.
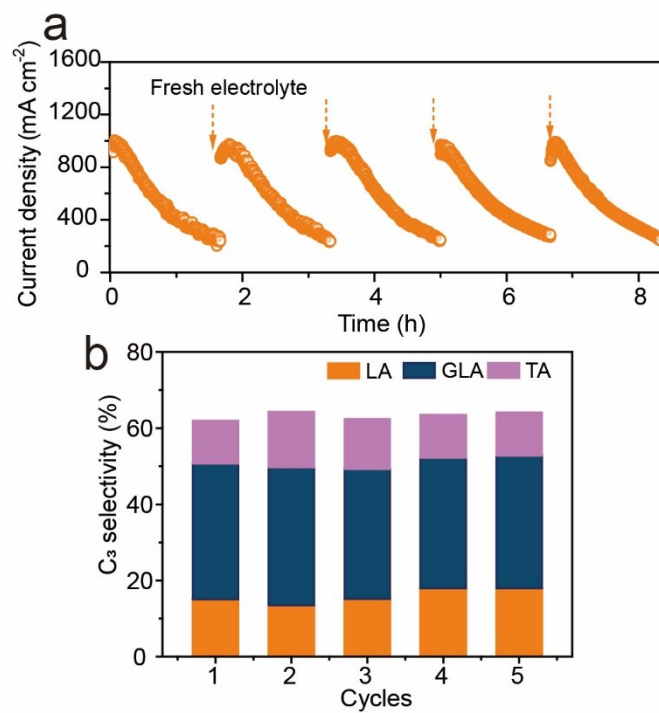
Figure S23. (a) I-t curves and (b) corresponding C_3 selectivity of hp-PtAu/NF for five successive electrolysis cycles at 1.6 V vs RHE.
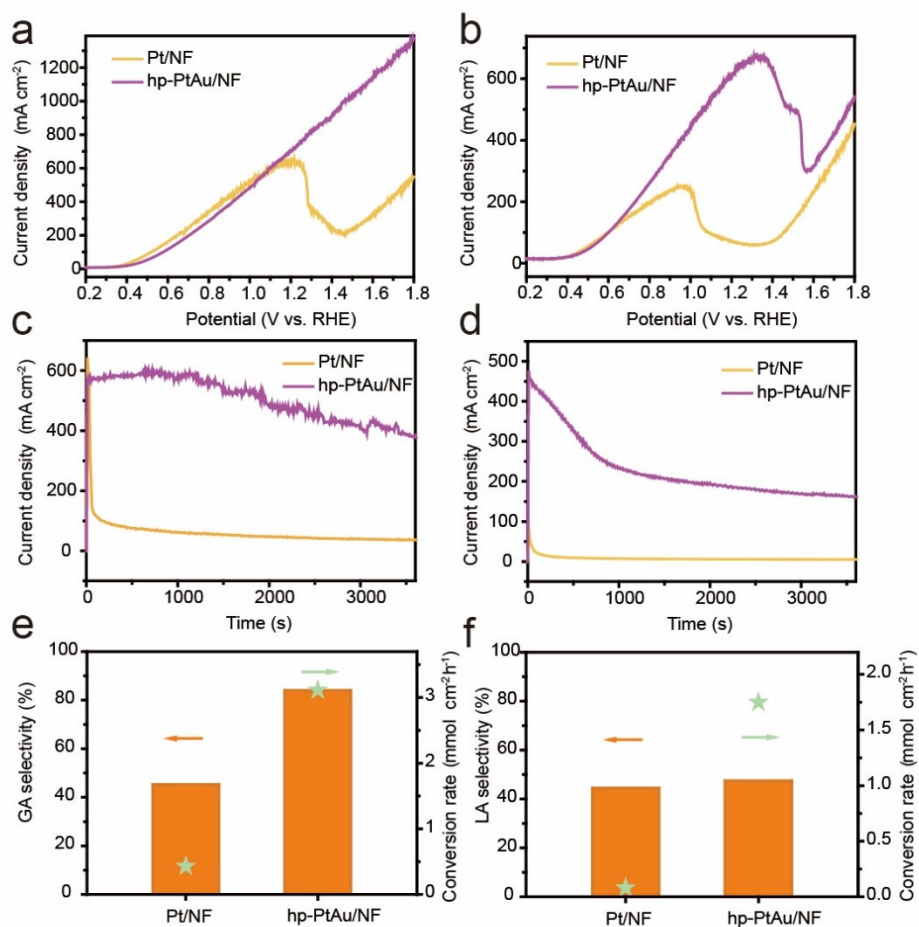
Figure S24. LSV curves of (a) ethylene glycol oxidation reaction (EGOR) and (b) 1,2-propanediol oxidation reaction (1,2-POR) catalyzed by Pt/NF and hp-PtAu/NF electrodes, respectively. I-t curves of (c) EGOR and (d) 1,2-POR catalyzed by Pt/NF and hp-PtAu/NF electrodes, respectively. (e) Ethylene glycol conversion rate and GA selectivity for Pt/NF and hp-PtAu/NF at 1.2 V vs. RHE. (f) 1,2-propanediol conversion rate and LA selectivity for Pt/NF and hp-PtAu/NF at 1.2 V vs. RHE.
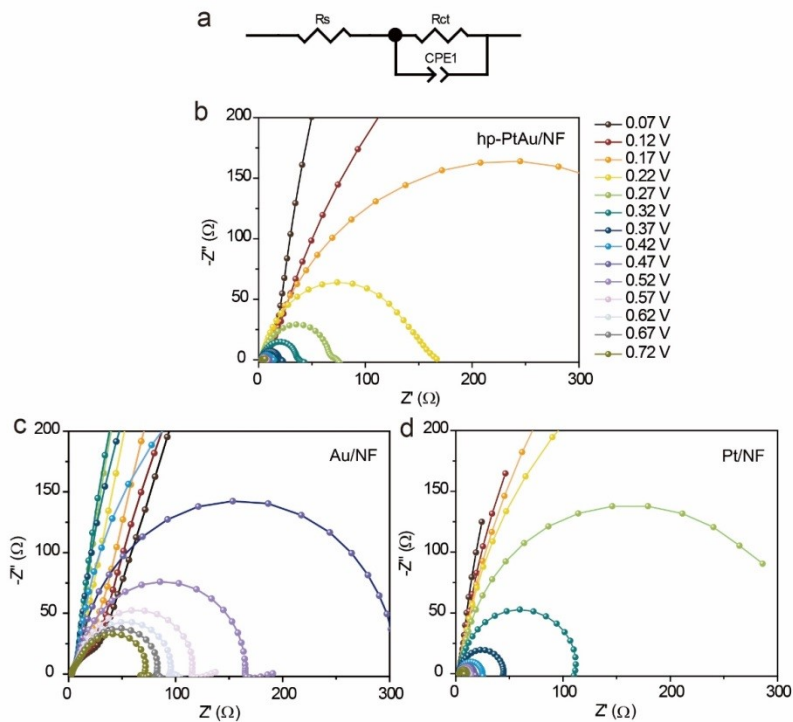
Figure S25. (a) The equivalent circuit diagram of the hp-PtAu/NF and Pt/NF samples. Nyquist plots of the (b) hp-PtAu/NF, (c) Au/NF and (d) Pt/NF in 1 M KOH with 0.5 M glycerol addition.
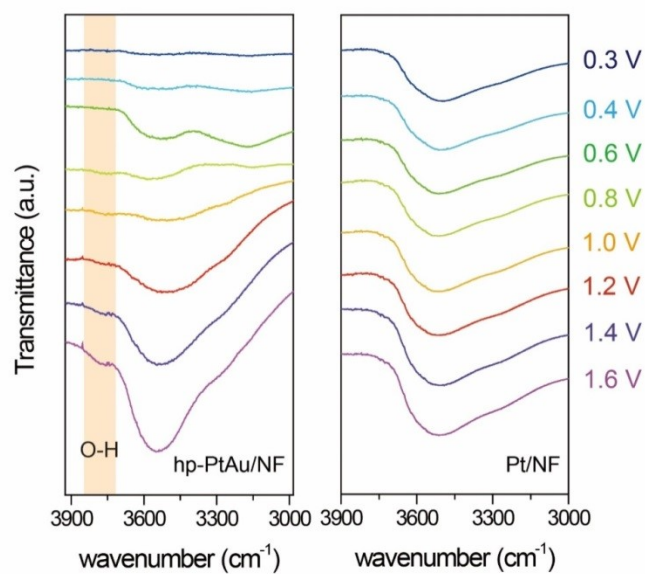
Figure S26. Electrochemical in situ FTIR spectra of hp-PtAu/NF and Pt/NF at different potentials in 1 M KOH containing 0.5 M glycerol.
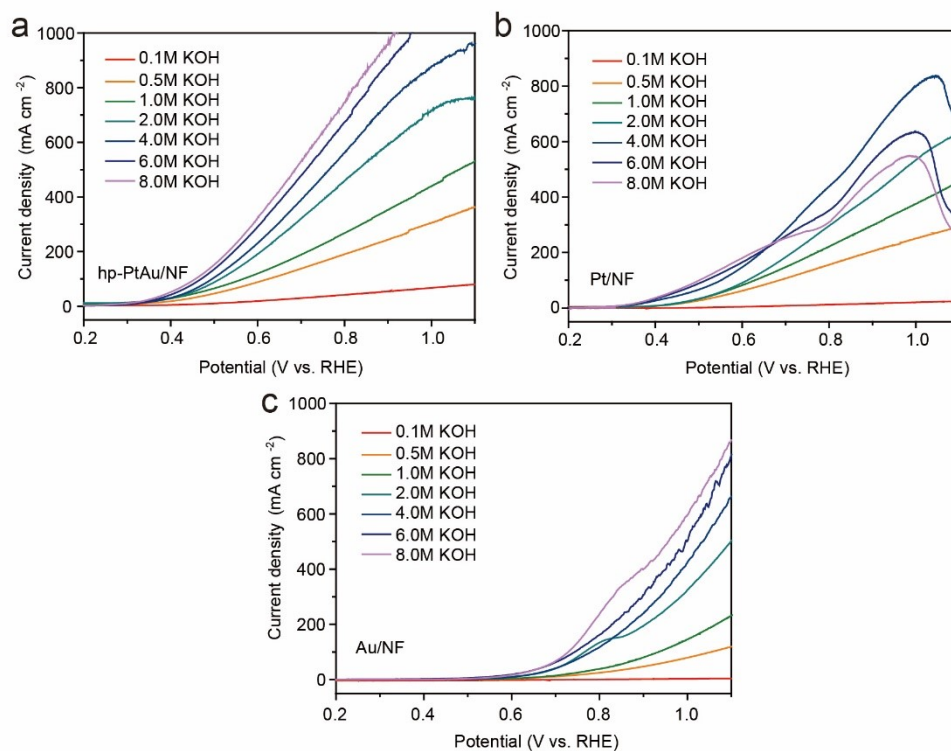
Figure S27. LSV curves of (a) hp-PtAu/NF, (b) Pt/NF and (c) Au/NF in KOH solutions of varied concentrations containing 0.5 M glycerol at a scan rate of 2 mV s^{-1}.
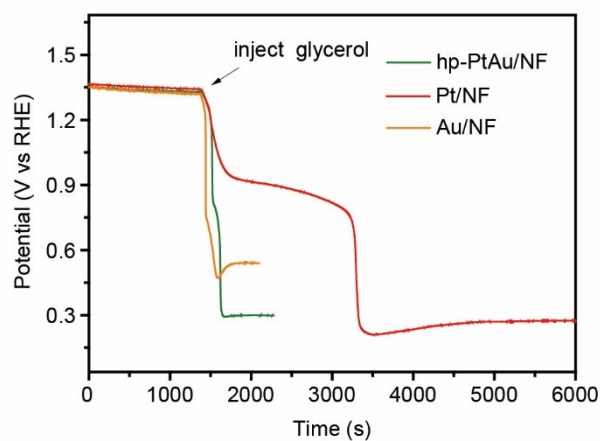
Figure S28. The OCP of the hp-PtAu/NF, Pt/NF and Au/NF samples in 1 M KOH electrolyte before and after glycerol was injected.
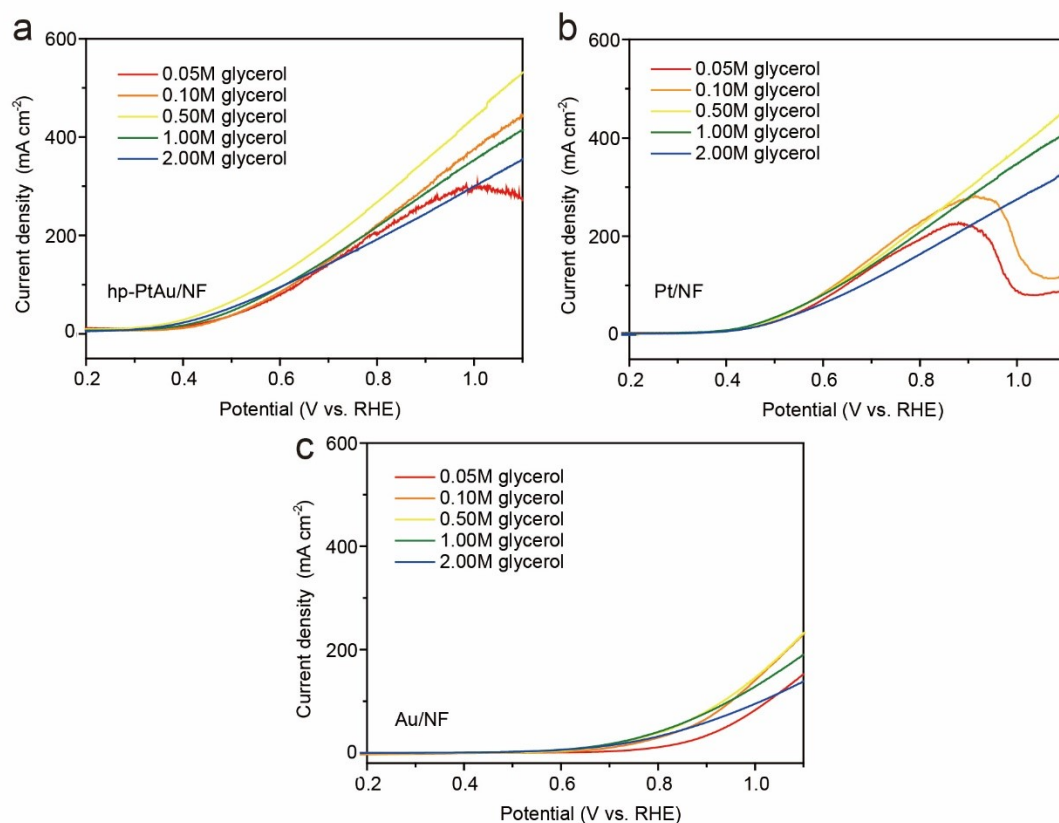
Figure S29. LSV curves of (a) hp-PtAu/NF, (b) Pt/NF and (c) Au/NF in 1M KOH solution with different concentrations of glycerol at a scan rate of 2 mV s^{-1}.
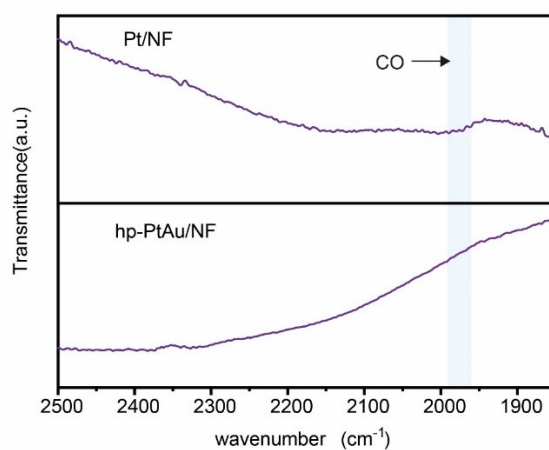
Figure S30. FTIR spectra of Pt/NF and hp-PtAu/NF at 1.6 V vs. RHE in 1 M KOH with 0.5 M glycerol.
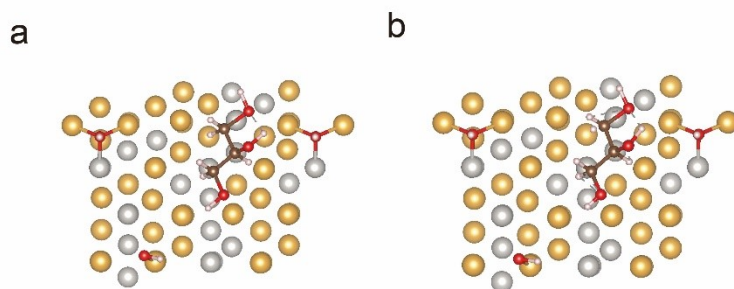
Figure S31. Molecular dynamics simulations of glycerol on PtAu surface at (a) 0 s, (b) 320 s.

$\Delta G_{OH^*}= -0.34$ eV $\Delta G_{OH^*}= -0.57$ eV $\Delta G_{OH^*}= -0.85$ eV

Number of OH*
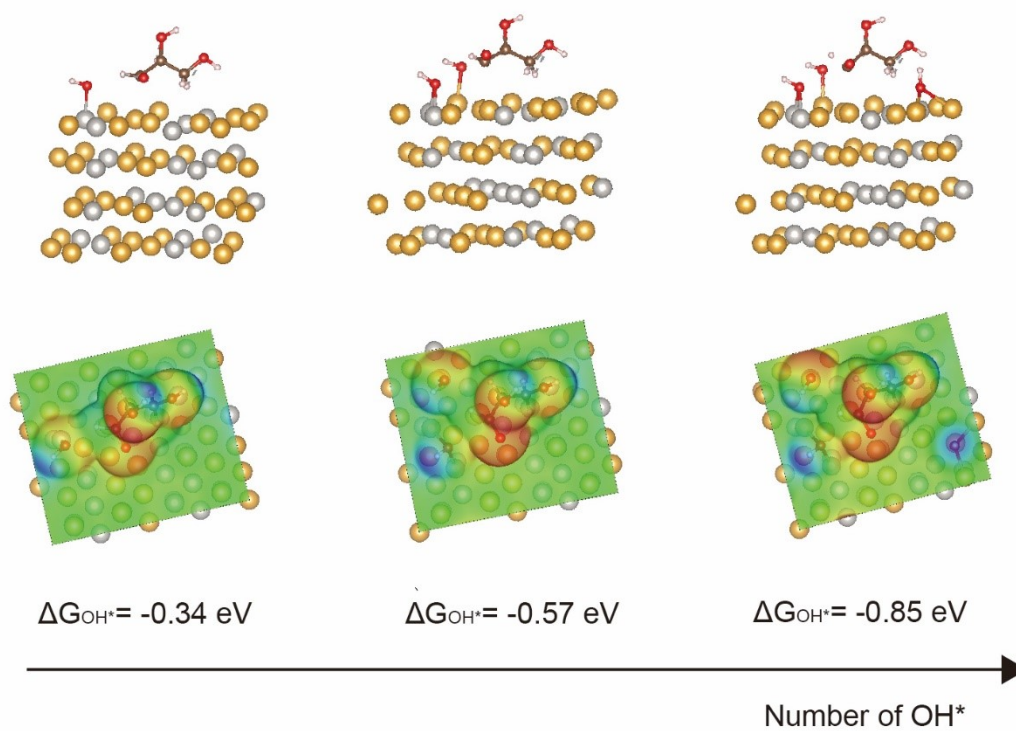
Figure S32. The Gibbs free formation energy (ΔG_{OH^*}) on PtAu alloy.
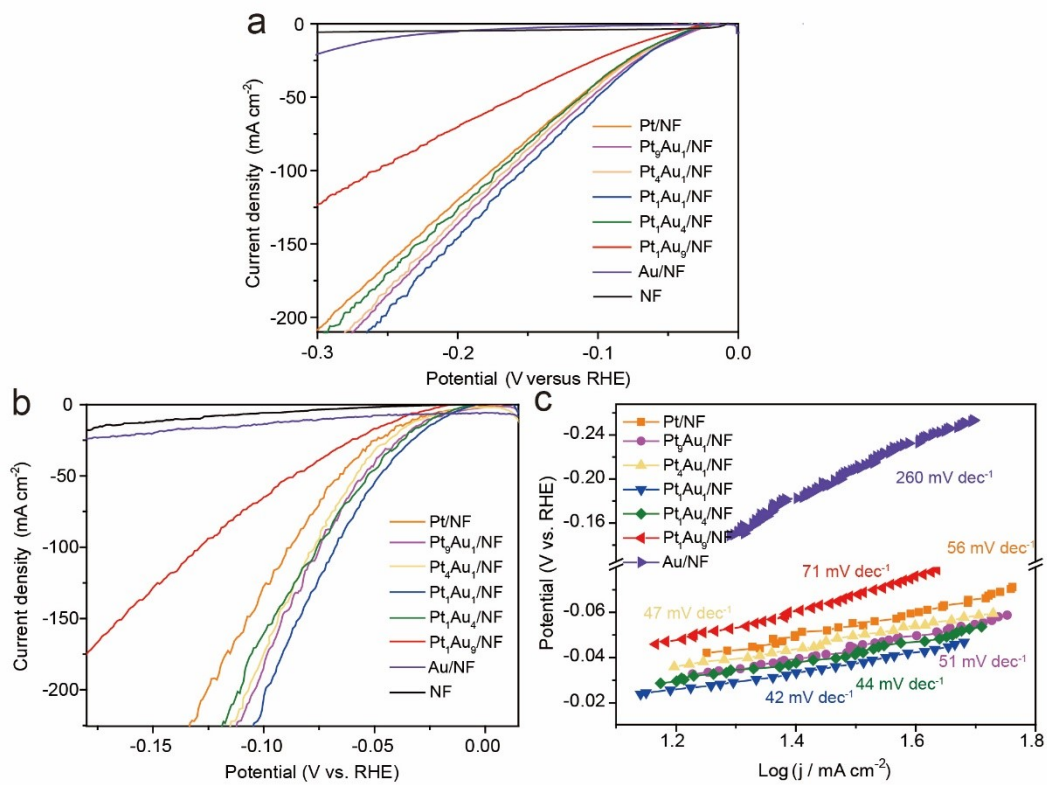
Figure S33. LSV curves of various catalysts for HER without (a) and with (b) *iR*-correction. (c) Corresponding Tafel slopes in 1 M KOH.
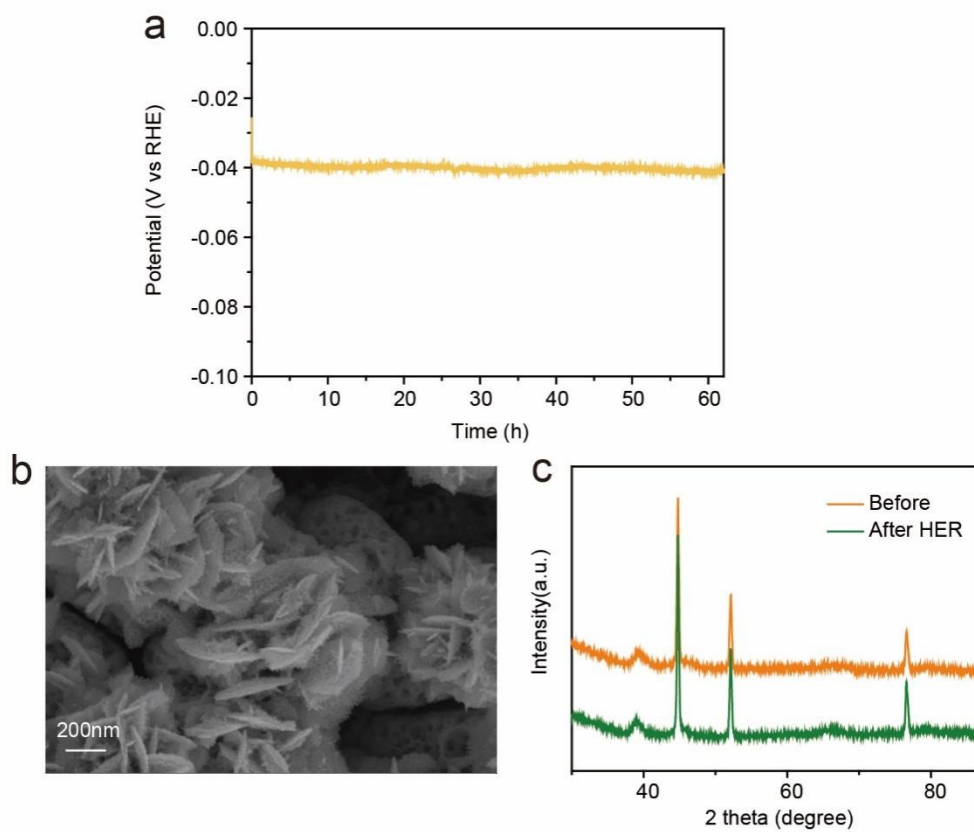
Figure S34. (a) Stability test of Pt_1Au_1/NF for cathodic HER at a current density of 10 mA cm^{-2}. (b) SEM and (c) XRD results of the cathodic Pt_1Au_1/NF catalyst after HER chronopotentiometric (CP) measurement.
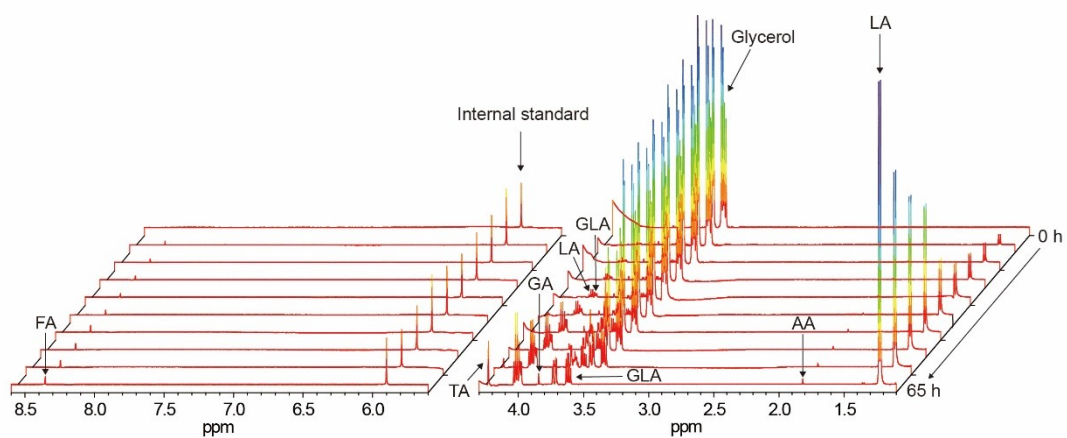
Figure S35. ^{1}H NMR spectra of the electrolyte after different reaction times (from 0 h - 65 h).
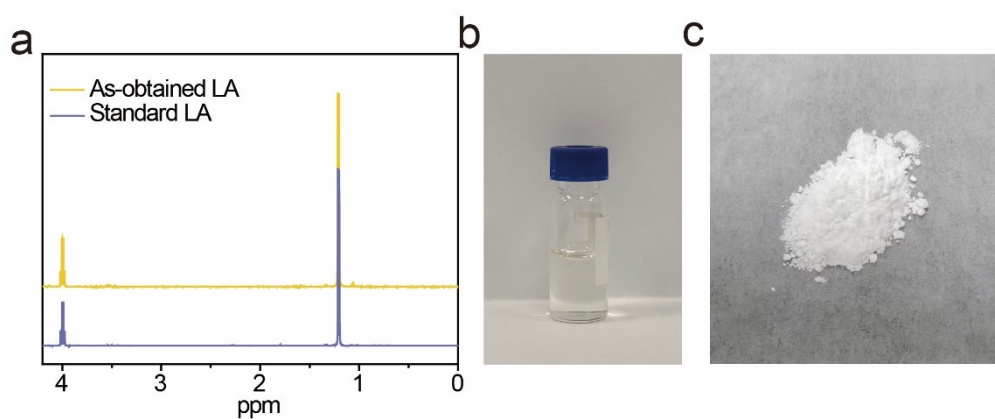
Figure S36. (a) ^{1}HNMR spectra of as-obtained LA and standard LA. Physical pictures of (b) as-obtained LA and (c) K$_2$SO$_4$ by rotary distillation.
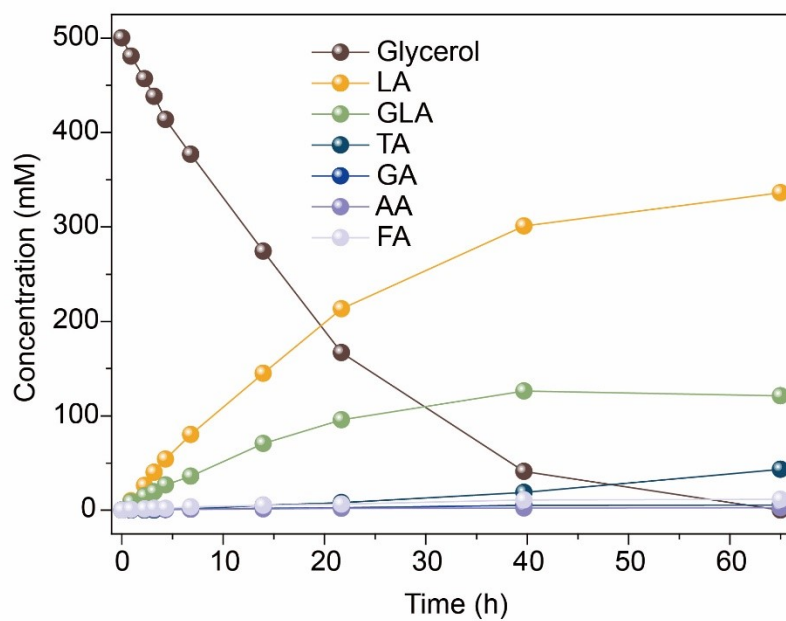
Figure S37. Concentrations of crude glycerol and its oxidation products as functions of time at a cell voltage of 0.5 V in the electrolyte of 1 M KOH with crude glycerol. Electrode area: 3 cm^2. Electrolyte volume: 20 mL.

$y = 175.51739 \, x + 1.53636$
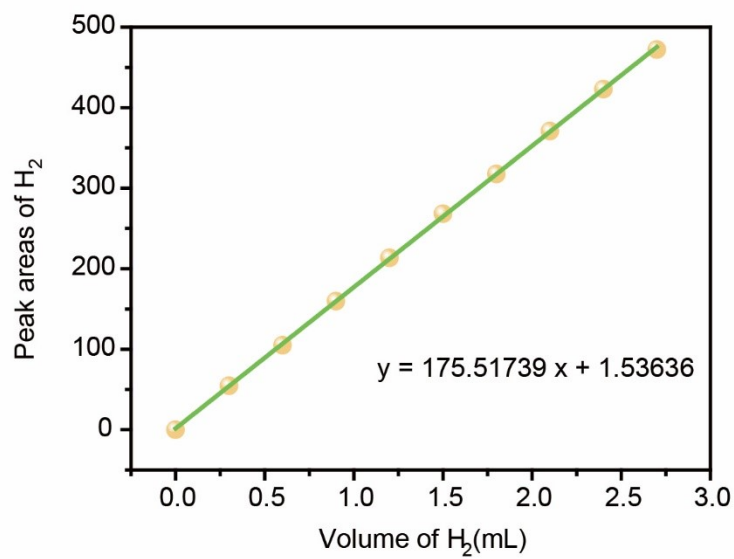
Figure S38. The standard curve of H_2 generation obtained by GC (N_2 as a carrier gas) and detected with thermal conductivity detector (TCD).

Supporting Tables

Table S1. Comparison of the electrochemical alcohol oxidation performances over Pt/Au-based catalysts reported in the literatures and in this work.

Catalyst	Substrate	Electrolyte	Reactant	Three-electrode system		Two-electrode system		Ref.
				Potential (V vs. RHE)	Current density (mA cm^{-2})	Voltage (V)	Current density (mA cm^{-2})	
Pt$_4$Au$_6$@Ag	GCE	0.1 M KOH	1 M glycerol	0.58	2.50			[6]
MoO$_x$/Pt	carbon fiber paper	1 M KOH	0.1 M glycerol			0.7	10	[7]
PtAg	glassy carbon	0.1 M KOH	1 M glycerol	0.51	onset			[8]
RA-Au	Ni foam	1 M KOH	0.1 M glycerol	~1.00	100			[9]
Au	carbon paper	0.1 M NaOH	0.1 M glycerol	1.00	10	1.20	~34	[10]
Au$_{50}$/Ag$_5$0-3.2M-PAA	carbon paper	1 M NaOH	0.1 M glycerol	1.21	83			[11]
Au/Ni(OH)$_2$	Ni foam	3 M KOH	0.3 M glycerol	0.95	317.7			[12]
Pt$_3$Ce/C	carbon paper	1 M KOH	1 M glycerol	1.48	10			[13]
Pt$_{0.95}$-Bi$_{0.05}$/TiN HNWs	carbon cloth	1 M KOH	0.05 M glycerol	0.7	25.4			[14]
Au$_3$Ag/C	carbon cloth	4 M KOH	1 M glycerol			~1.05	100	[15]
Au/CoOOH	Ni foam	1 M KOH	0.1 M benzyl alcohol	1.50	540	1.60	~80	[16]
hp-PtAu	**Ni foam**	**1 M KOH**	**0.5 M glycerol**	0.26	10	0.3	10	**This work**
				0.9	352	1.05	300	
		4 M KOH		0.9	746			

Table S2. Comparison of the electrochemical alcohol oxidation performances in the literatures and in this work.

Catalyst	Substrate	Electrolyte	Reactant	Three-electrode system		Two-electrode system		Ref.
				Potential (V vs. RHE)	Current density (mA cm^{-2})	Voltage (V)	Current density (mA cm^{-2})	
Ni$_{80}$Pd$_{20}$	glassy carbon	1 M KOH	0.1 M glycerol	1.21	onset			[17]
Pd-NCs/NiO-uNPs	GCE	1 M KOH	0.5 M glycerol	1.43	100	1.62	10	[18]
Ni-Mo-N/CFC	Carbon fiber cloth	1 M KOH	0.1 M glycerol	1.30	10	1.36	10	[19]
CuCo-oxide	Ni foam	0.1 M KOH	0.1 M glycerol	1.25	10			[20]
NiCo$_2$O$_4$	Ni foam	1 M NaOH	0.1 M glycerol	1.23	10	1.35	10	[21]
Ni$_3$N/Co$_3$N-NWs	Ni foam	1 M KOH	0.1 M glycerol	1.18	20	1.47	50	[22]
S-CuO		1 M KOH	0.1 M glycerol	1.23	100	1.37	100	[23]
Pd/C-CeO$_2$	GCE	2 M KOH	2 M 1, 3-propanediol	-	-	1.00	70	[24]
PdBi	Ni foam	1.5 M KOH	1 M 1, 3-propanediol	~0.76	200	0.86	20	[25]
PdAg	Ni foam	0.5 M KOH	1 M ethylene glycol	0.57	10	1.02	20	[26]
Mo–Ni alloy	Ni foam	1 M KOH	0.01M Benzyl alcohol	1.35	15	1.53	100	[27]
Co(OH)2@HOS	carbon paper	1 M KOH	3 M methanol	1.385	10	1.497	10	[28]
hp-PtAu	Ni foam	1 M KOH	0.5 M glycerol	0.26	10	0.3	10	This work
				0.9	352	1.05	300	
		4 M KOH		0.9	746			

Table S3. Comparison of the C_3 products for electrochemical glycerol oxidation in the literatures and in this work.

Catalyst	Substrate	Electrolyte	Reactant	C_3 products selectivity (%)	Ref.
MoO$_x$/Pt	carbon fiber paper	1 M KOH	0.1 M glycerol	80 (GLA 73, TA 7)	7
Pt-CC	carbon cloth	2 M KOH	4 M glycerol	75 (GLA 41, LA 34)	29
Pt-in-VGCC	carbon cloth	1 M KOH	0.1 M glycerol	78 (GLA 43, TA 5, DHA 30)	30
Pt/C	GCE	0.5 M H$_2$SO$_4$	53.1 mM glycerol	76.1 (GLD 29.4, DHA 5.8, GLA 40.9)	31
Pt–CeO$_2$/GNS	GCE	0.1 M KOH	1 M glycerol	62 (GLA ~10, GLD 52)	32
Pt$_{1-x}$-Bi$_x$/TiN HNWs	carbon cloth	1 M KOH	0.05 M glycerol	75.6 (GLA 36.6, LA 14.5, TA 24.5)	14
Pt$_4$Au$_6$@Ag	GCE	0.1 M KOH	1 M glycerol	90.44 (TA 0.04, GLA 7.3, GLD 6.9, DHA 76.2)	6
CuAu/C	carbon cloth	0.5 M NaOH	0.5 M glycerol	53.58 (GLA 39.03, TA 14.55)	33
Au/Ni(OH)$_2$	Ni foam	3 M KOH	0.3 M glycerol	87.8 (TA 2.3, GLA 10.5, LA 75)	12
ALD(TiO$_2$)-Au/C	Carbon paper	0.1 M KOH	0.1 M glycerol	76.1 (GLA 64.9, HPA 6.4, TA 4.8)	34
hp-PtAu	**Ni foam**	**1 M KOH**	**0.5 M glycerol**	**95 (LA 70%, GLA 25)**	**This work**

Table S4. The related EIS fitting parameters of hp-PtAu/NF sample for GOR.

Potential（vs RHE）	Rs （Ω）	Rct （Ω）	CPE1-T	CPE1-P
0.17	2.787	465.2	0.0057	0.8051
0.22	2.816	153.4	0.0039	0.8730
0.27	2.811	67.19	0.0036	0.8812
0.32	2.802	34.27	0.0033	0.8884
0.37	2.795	16.92	0.0030	0.8987
0.42	2.797	9.541	0.0029	0.8960
0.47	2.818	6.331	0.0030	0.8877
0.52	2.845	4.403	0.0031	0.8745
0.57	2.87	3.317	0.0033	0.8593
0.62	2.898	2.609	0.0033	0.8545
0.67	2.92	2.258	0.0035	0.8426
0.72	2.952	2.041	0.0037	0.8320

Table S5. The related EIS fitting parameters of Pt/NF sample for GOR.

Potential（vs RHE）	Rs（Ω）	Rct（Ω）	CPE1-T	CPE1-P
0.27	3.125	332.7	0.0164	0.9002
0.32	3.133	116.6	0.0138	0.9230
0.37	3.124	43.02	0.0130	0.9284
0.42	3.145	21.99	0.0130	0.9248
0.47	3.155	14.39	0.0133	0.9204
0.52	3.172	10.81	0.0129	0.9499
0.57	3.174	8.829	0.0142	0.9009
0.62	3.211	8.26	0.0140	0.9017
0.67	3.223	7.87	0.0135	0.9125
0.72	3.245	7.397	0.01132	0.9159

Table S6. The related EIS fitting parameters of Au/NF sample for GOR.

Potential（vs RHE）	Rs（Ω）	Rct（Ω）	CPE1-T	CPE1-P
0.32	7.663	3728	0.0011	0.9462
0.37	7.607	1751	0.0010	0.9512
0.42	7.062	709.7	0.0009	0.9454
0.47	7.767	301.5	0.0009	0.9603
0.52	7.373	160.7	0.0008	0.9552
0.57	7.382	110.7	0.0008	0.9585
0.62	7.156	92.17	0.0008	0.9439
0.67	7.16	79.58	0.0008	0.9473
0.72	8.587	64.85	0.0007	1.001

Supporting References

[1] F. Wang, L. Ju, B. Wu, S. Li, J. Peng, Y. Chen, M. Getaye Sendeku, K. Wang, Y. Cai, J. Yi, Y. Yang, Z. Wang, X. Sun, *Angew. Chem. Int. Ed.* 2024, 63, e202402033.

[2] G. Kresse, J. Furthmuller, Efficient iterative schemes for ab initio total-energy calculations using a plane-wave basis set. *Phys. Rev. B* **1996**, *54*, 11169-11186.

[3] J. P. Perdew, K. Burke, M. Ernzerhof, Generalized Gradient Approximation Made Simple. *Phys. Rev. Lett.* **1996,** *77*, 3865.

[4] W. G. Hoover Phys. Rev. A **1985**, 31, 1695-1697.

[5] Kira. Mathew, R. Sundararaman, K. Letchworth-Weaver, T. A. Arias, R. G. Hennig, *J. Chem. Phys*. **2014**; 140 (8): 084106.

[6] Y. Zhou, Y. Shen, J. Xi, *Appl. Catal., B* **2019**, *245*, 604-612.

[7] X. Yu, E. C. Dos Santos, J. White, G. Salazar-Alvarez, L. G. M. Pettersson, A. Cornell, M. Johnsson, *Small* **2021**, *17*, e2104288.

[8] Y. Zhou, Y. Shen, J. Xi, X. Luo, *ACS Appl. Mater. Interfaces* **2019**, *11*, 28953-28959.

[9] D. Kim, L. S. Oh, Y. C. Tan, H. Song, H. J. Kim, J. Oh, *ACS Catal.* **2021**, *11*, 14926-14931.

[10] Y. Xie, L. Sun, X. Pan, Z. Zhou, Y. Zheng, X. Yang, G. Zhao, *Carbon* **2023**, *203*, 88-96.

[11] N. Tuleushova, A. Amanova, I. Abdellah, M. Benoit, H. Remita, D. Cornu, Y. Holade, S. Tingry, *Nanomaterials* **2023**, *13*, 1713.

[12] Y. Yan, H. Zhou, S. M. Xu, J. Yang, P. Hao, X. Cai, Y. Ren, M. Xu, X. Kong, M. Shao, Z. Li, H. Duan, *J. Am. Chem. Soc.* **2023**, *145*, 6144-6155.

[13] Y. Hai, Y. Chang, J. Jia, A. Xu, M. Jia, *Int. J. Hydrogen Energy* **2023**, *48*, 14742-14748.

[14] L. Liu, B. Liu, X. Xu, P. Jing, J. Zhang, *J. Power Sources* **2022**, *543*, 231836.

[15] J. B. Costa Santos, C. Vieira, R. Crisafulli, J. J. Linares, *Int. J. Hydrogen Energy* **2020**, *45*, 25658-25671.

[16] Z. Li, Y. Yan, S. M. Xu, H. Zhou, M. Xu, L. Ma, M. Shao, X. Kong, B. Wang, L. Zheng, H. Duan, *Nat. Commun.* **2022**, *13*, 147.

[17] M. S. E. Houache, K. Hughes, A. Ahmed, R. Safari, H. Liu, G. A. Botton, E. A. Baranova, *ACS Sustain. Chem. Eng.* **2019**, *7*, 14425-14434.

[18] G. Ma, N. Yang, G. Zhou, X. Wang, *Nano Research* **2021**, *15*, 1934-1941.

[19] Y. Li, X. Wei, L. Chen, J. Shi, M. He, *Nat. Commun.* **2019**, *10*, 5335.

[20] L. S. Oh, M. Park, Y. S. Park, Y. Kim, W. Yoon, J. Hwang, E. Lim, J. H. Park, S. M. Choi, M. H. Seo, W. B. Kim, H. J. Kim, *Adv. Mater.* **2023**, *35*. 2203285.

[21] G. Wu, X. Dong, J. Mao, G. Li, C. Zhu, S. Li, A. Chen, G. Feng, Y. Song, W. Chen, W. Wei, *Chem. Eng. J.* **2023**, *468*,143640.

[22] Y. Zhu, Q. Qian, Y. Chen, X. He, X. Shi, W. Wang, Z. Li, Y. Feng, G. Zhang, F. Cheng, *Adv. Funct. Mater.* **2023**, *33*, 2300547.

[23] R.-Y. Fan, X.-J. Zhai, W.-Z. Qiao, Y.-S. Zhang, N. Yu, N. Xu, Q.-X. Lv, Y.-M. Chai, B. Dong, *Nano-Micro Letters* **2023**, *15,*190.

[24] J. Mahmoudian, M. Bellini, M. V. Pagliaro, W. Oberhauser, M. Innocenti, F.

Vizza, H. A. Miller, *ACS Sustain. Chem. Eng.* **2017**, *5*, 6090-6098.

[25] D. Si, M. Wang, X. Yang, C. Wang, K. Shi, B. Huang, L. Chen, J. Shi, *Appl. Catal., B* **2023**, *331*, 122664.

[26] D. Si, B. Xiong, L. Chen, J. Shi, *Chem Catal.* **2021**, *1*, 941-955.

[27] X. Cui, M. Chen, R. Xiong, J. Sun, X. Liu, B. Geng, *J. Mater. Chem. A* **2019**, *7*, 16501-16507.

[28] K. Xiang, D. Wu, X. Deng, M. Li, S. Chen, P. Hao, X. Guo, J. L. Luo, X. Z. Fu, *Adv. Funct. Mater.* **2020**, *30*, 1909610.

[29] H. Yadegari, A. Ozden, T. Alkayyali, V. Soni, A. Thevenon, A. Rosas-Hernández, T. Agapie, J. C. Peters, E. H. Sargent, D. Sinton, *ACS Energy Lett.* **2021**, *6*, 3538-3544.

[30] Z. Chen, C. Liu, X. Zhao, H. Yan, J. Li, P. Lyu, Y. Du, S. Xi, K. Chi, X. Chi, H. Xu, X. Li, W. Fu, K. Leng, S. J. Pennycook, S. Wang, K. P. Loh, *Adv. Mater.* **2019**, *31*, e1804763.

[31] H. Sheng, A. N. Janes, R. D. Ross, H. Hofstetter, K. Lee, J. R. Schmidt, S. Jin, *Nat. Catal.* **2022**, *5*, 716-725.

[32] W. Chen, Y. Zhou, Y. Shen, *Electrochemistry* **2019**, *87*, 30-34.

[33] L. Thia, M. Xie, Z. Liu, X. Ge, Y. Lu, W. E. Fong, X. Wang, *ChemCatChem* **2016**, *8*, 3272-3278.

[34] J. Han, Y. Kim, D. H. K. Jackson, K.-E. Jeong, H.-J. Chae, K.-Y. Lee, H. J. Kim, *Electrochem. Commun.* **2018**, *96*, 16-21.